Cite as: X. Chi *et al.*, *Science* 10.1126/science.abc6952 (2020).

A neutralizing human antibody binds to the N-terminal domain of the Spike protein of SARS-CoV-2

Xiangyang Chi[1]*, Renhong Yan[2]*, Jun Zhang[1]*, Guanying Zhang[1], Yuanyuan Zhang[2], Meng Hao[1], Zhe Zhang[1], Pengfei Fan[1], Yunzhu Dong[1], Yilong Yang[1], Zhengshan Chen[1], Yingying Guo[2], Jinlong Zhang[1], Yaning Li[3], Xiaohong Song[1], Yi Chen[1], Lu Xia[2], Ling Fu[1], Lihua Hou[1], Junjie Xu[1], Changming Yu[1], Jianmin Li[1]†, Qiang Zhou[2]†, Wei Chen[1]†

[1]Beijing Institute of Biotechnology, Academy of Military Medical Sciences (AMMS), Beijing 100071, China. [2]Key Laboratory of Structural Biology of Zhejiang Province, Institute of Biology, Westlake Institute for Advanced Study, School of Life Sciences, Westlake University, Hangzhou 310024, Zhejiang Province, China. [3]Beijing Advanced Innovation Center for Structural Biology, Tsinghua-Peking Joint Center for Life Sciences, School of Life Sciences, Tsinghua University, Beijing 100084, China.

***These authors contributed equally to this work.**

†Corresponding author. Email: cw0226@foxmail.com (W.C.); zhouqiang@westlake.edu.cn (Q.Z.); lijmqz@126.com (J.L.)

Developing therapeutics against SARS-CoV-2 could be guided by the distribution of epitopes, not only on the receptor binding domain (RBD) of the Spike (S) protein, but also across the full Spike (S) protein. We isolated and characterized monoclonal antibodies (mAbs) from ten convalescent COVID-19 patients. Three mAbs showed neutralizing activities against authentic SARS-CoV-2. An mAb, named 4A8, exhibits high neutralization potency against both authentic and pseudotyped SARS-CoV-2, but does not bind the RBD. We defined the epitope of 4A8 as the N terminal domain (NTD) of the S protein by determining its cryo-EM structure in complex with the S protein to an overall resolution of 3.1 Angstrom and local resolution of 3.3 Angstrom for the 4A8-NTD interface. This points to the NTD as a promising target for therapeutic mAbs against COVID-19.

The global outbreak of COVID-19 has emerged as a severe threat to human health (*1–3*). COVID-19 is caused by a novel coronavirus, the severe acute respiratory syndrome coronavirus 2 (SARS-CoV-2), which is an enveloped, positive-strand RNA virus that causes symptoms such as cough, headache, dyspnea, myalgia, fever and severe pneumonia in humans (*1*, *3–5*).

SARS-CoV-2 is a member of the β coronavirus genus, which also contains SARS-CoV and MERS-CoV that caused epidemic in 2002 and 2012, respectively (*6*, *7*). SARS-CoV-2 shares about 80% sequence identity to SARS-CoV and uses the same cellular receptor, angiotensin-converting enzyme 2 (ACE2) (*8–16*).

The trimeric S protein decorates the surface of coronavirus and plays a pivotal role during viral entry (*17*, *18*). During infection the S protein is cleaved into the N-terminal S1 subunit and C-terminal S2 subunit by host proteases such as TMPRSS2 (*18*, *19*) and changes conformation from the prefusion to the postfusion state (*20*). S1 and S2 comprises the extracellular domain (ECD, 1-1208 amino acids) and a single transmembrane helix and mediate receptor binding and membrane fusion, respectively (*16*). S1, consisting of the N-terminal domain (NTD) and the receptor binding domain (RBD), is critical in determining tissue tropism and host ranges (*21*, *22*). The RBD is responsible for binding to ACE2, while the function of NTD is not well understood. In some coronaviruses, the NTD may recognize specific sugar moieties upon initial attachment and might play an important role in the prefusion to postfusion transition of the S protein (*23–26*). The NTD of the MERS-CoV S protein can serve as a critical epitope for neutralizing antibodies (*26*).

The SARS-CoV-2 S protein-targeting monoclonal antibodies (mAbs) with potent neutralizing activity are a focus in developing therapeutic interventions for COVID-19 (*27–29*). Many studies reported the functions and structures of SARS-CoV-2 neutralizing antibodies that target the RBD and inhibit the association between the S protein and ACE2 (*28–34*). The RBD-targeting antibodies applied individually, might induce resistance mutations in the virus (*26*). Antibodies targeting non-RBD epitopes might be added to antibody cocktail therapeutics for SARS-CoV-2. We thus sought to identify antibodies to different regions of the S protein and to the Nucleocapsid (N) protein.

Results

Isolation of human mAbs from memory B cells and plasma B cells

To isolate monoclonal antibodies and analyze the humoral antibody responses to SARS-CoV-2, we collected plasma and peripheral blood mononuclear cells (PBMCs) from 10 Chinese patients recovered from SARS-CoV-2 infection. The age of donors ranges from 25 to 53 years. The interval from disease confirmation date to blood collection date ranged from 23 to 29 days for patients 1-5, and 10 to 15 days

for patients 6-10 (table S1). We evaluated the titers of binding antibodies in plasma to different fragments of the SARS-CoV-2 S protein, including the full ECD, S1, S2, and the RBD; and to the Nucleocapsid (N) Protein. Plasma from all the patients except donor 2 bound to all 5 SARS-CoV-2 protein segments, while that from donor 2 recognized S-ECD and S2 only (Fig. 1A). The neutralizing capacities of plasma against authentic SARS-CoV-2 and HIV-vectored pseudotyped SARS-CoV-2 are correlated ($r=0.6868$, $p<0.05$) (Fig. 1B). These results indicate that humoral immune responses were specifically elicited for all of the 10 patients during their natural infection with SARS-CoV-2.

To isolate S protein-specific monoclonal antibodies, we first sorted the IgG^+ memory B cells from peripheral blood mononuclear cells (PBMCs) of convalescent patients 1-5 with flow cytometry using S-ECD as probe (Fig. 1C). The percentage of S-ECD-reactive IgG^+ B cells ranges from 0.56% to 11% as revealed by fluorescence activating cell sorter (FACS). To avoid losing B cells with low copies of S-ECD-specific receptors on cell surfaces, we sorted plasma B cells from mixed PBMCs derived from another five convalescent patients (patient 6-10) without using S-ECD protein as probe in flow cytometry. The percentage of plasma B cells in CD3-CD19+ B cells was 12.8%, which is higher than the percentage of memory B cells in CD3-$CD19^+$ B cells (Fig. 1C).

From the sorted B cells, we identified 9, 286, 43, 12 and 26 clones of single B cell from patients 1 to 5, respectively, and 23 clones of single B cell from the mixed PBMCs of patients 6 to 10 (Fig. 1D). The distribution of the sequenced heavy (IgH) gene families was comparable among the 10 donors, with VH3 being the most commonly used VH gene, while different donors displayed variable preferences for the light chain (IgL) gene families (Fig. 1D). The combination of V3 and J4, V3 and D3, and D3 and J4 were the most common usage for the IgH gene family (fig. S1). The average mutations of amino acids per mAb from memory B cells ranged from 17.50 to 48.04 for donor 1 to 5, respectively, while mAbs from plasma B cells possessed an average of 13.99 amino acid mutations for donor 6 to 10 (Fig. 1E). Human antibodies elicited by repeated exposures to different antigens confer an average of 26.46 amino acid mutations per Ab, as previously reported (*35*). These results indicate that natural SARS-CoV-2 infection elicited high levels of somatic hypermutation (SHM) in memory B cells. The lengths of complementarity-determining region (CDR) 3 for antibodies were similar among the donors, with average lengths of these CDR3 ranging from 13.9 to 17.7 for VH and 9.3 to 10.1 for VL (Fig. 1F). Notably, the CDR3 lengths of these mAbs were longer than that in antigen-specific immune receptors (means of 12.7 for VH and 6.5 for VL, respectively) reported previously (*36*).

Binding profiles of SARS-CoV-2 S protein-specific human mAbs

To screen for S protein-specific antibodies, we determined the binding specificity using enzyme linked immunosorbent assay (ELISA) for the 399 human mAbs sorted above. 1, 16, 1, 3, and 9 S-ECD-specific mAbs were identified from donors 1-5, respectively. A total of 35 S-ECD-specific mAbs were identified from donors 6 -10 (Fig. 2A). We further characterized domain specificities of the 35 mAbs with different fragments of the S protein, including S1, S2 and RBD (Fig. 2A). The S-reactive mAbs are classified into 4 major groups based on their EC_{50} values (Fig. 2A). Group 1 recognizes only S-ECD. Group 2 recognizes S-ECD and S1, with subgroup 2A binding S-ECD and S1 and subgroup 2B binding S-ECD, S1, and RBD. Group 3 interacts with both S1 and S2, where subgroup 3A targets the RBD and subgroup 3B fails to bind the RBD. Group 4 recognizes S-ECD and S2. Remarkably, only 4 mAbs recognize the RBD among the 35 S-specific mAbs (Fig. 2, A and B).

A competition-binding assay using ELISA was performed for several representative mAbs to determine if there are overlapping antigenic sites between different mAbs, with CR3022 being used as a positive control mAb that reported to bind the SARS-CoV-2 RBD (Fig. 2C) (*37*). Among these mAbs, 4A8 in group 2A competed with 1M-1D2 in group 2B. Another RBD-reactive mAb, 2M-10B11 in group 2B, competed with CR3022, suggesting overlapped epitopes on RBD for these two mAbs. These results indicate that antibody responses elicited by natural SARS-CoV-2 infection were diverse in epitope recognition of S proteins.

To characterize the diversity in gene usage and affinity maturation, the phylogenetic trees of these S-ECD-specific mAbs were analyzed based on the amino acid sequences of VHDJH and VLJL using a neighbor-joining method in MEGA7 Software (*38*). Results indicate that the VH gene usage is very diverse among the 35 mAbs from 10 donors, with VH 3-30 being the most frequently used germline gene. There was no particularly favored VH gene identified among S1, S2, or RBD-reactive mAbs (Fig. 2D). The percentages of heavy chain variable gene sequence identity ranged from 40.9% to 97.6% in the 35 S-ECD-specific mAb (fig. S2 and table S2).

Neutralizing activities of SARS-CoV-2 S-specific human mAbs

We first performed in vitro neutralization studies of the 35 S-ECD-specific mAbs using authentic SARS-CoV-2 in Vero-E6 cells (Fig. 3A). Of the 35 S-ECD-specific mAbs, only 3 mAbs neutralized authentic SARS-CoV-2. MAb 1M-1D2, 4A8, and 0304-3H3 exhibited medium to high neutralizing capacity with medium effective concentration (EC_{50}) at 28, 0.61, and 0.04 μg/ml, respectively. As expected, the RBD-targeting control mAb, CR3022, failed to neutralize authentic SARS-CoV-2

(*37*). Moreover, while the CR3022-competing mAb, 2M-10B11, bound to the SARS-CoV-2 RBD with EC_{50} of 5 ng/ml (Fig. 2A), it also failed to neutralize authentic SARS-CoV-2. These results suggest that binding affinities of mAbs against RBD do not correlate fully with the neutralizing abilities of mAbs. To further investigate the inhibitory activity of the 3 authentic SARS-CoV-2-neutralizing mAbs, 4A8, 0304-3H3, and 1M-1D2, we tested the RNA load of authentic SARS-CoV-2 in Vero-E6 cells treated with each mAb using real time qPCR (Fig. 3B). Consistent with the cytopathic effect (CPE) assay results (Fig. 3A), mAb 0304-3H3 and 4A8 displayed higher inhibitory capacities than 1M-1D2 (Fig. 3B).

We next performed luciferase reporter gene assays for all 35 S-binding mAbs using HIV-vectored pseudotyped SARS-CoV-2 (*39*), among which 3 mAbs exhibited neutralizing activity against the pseudotyped virus (Fig. 3C). 4A8 protected ACE2-293T cells with EC_{50} of 49 μg/ml. Although mAb 2M-10B11 and 9A1 did not neutralize authentic SARS-CoV-2, 2M-10B11 protected against pseudotyped virus with EC50 of 170 μg/ml and 9A1 provided weak protection. To our surprise, neutralization by 0304-3H3 and 1M-1D2 was not observed (Fig. 3C). The inconsistency between the results for pseudotyped SARS-CoV-2 compared to authentic SARS-CoV-2 were also observed for mAbs against MERS-CoV (*40*, *41*), and may be caused by the different presentation of S protein resulted from the difference environmental factors the viruses underwent, such as the cells used for the neutralizing assays or for the production of the pseudotyped or authentic virions (*42*). Based on these results, 4A8 is a potential candidate for the treatment of SARS-CoV-2, because it displayed strong neutralizing capacities against both authentic and pseudotyped SARS-CoV-2.

Binding characterization of candidate mAbs

To determine the possible neutralizing mechanism of the mAbs, we determined the binding affinities of the 5 mAbs with potential neutralizing activity against different segments of the S protein, including the full S-ECD, and domains S1, S2, and RBD using bio-layer interferometry. All 5 tested mAbs bound to S-ECD with high affinity- equilibrium dissociation constants (K_D) less than 2.14 nM (Fig. 4A). 4A8 and 1M-1D2 bound to S1 with K_D of 92.7 nM and 108 nM, respectively, whereas 0304-3H3 and 9A1 targeted S2 with K_D of 4.52 nM and < 0.001 nM, respectively (Fig. 4A, lower panels). Moreover, 2M-10B11 bound the RBD with K_D of 24.3 nM, which was obtained using heterogeneous ligand model due to the avidity effects (Fig. 4A, lower panels).

To investigate whether these mAbs block the binding of S protein to ACE2, we performed flow cytometry using HEK 293T cells expressing human ACE2. As expected, only 2M-10B11 among the 5 mAbs and ACE2-Fc prevented S protein from binding to ACE2. In the presence of 2M-10B11 only of 0.52% of cells were double positive for IgG and (Fig. 4B). CR3022, which competes with 2M-10B11, did not significantly block the binding of S to ACE2. The control mAb 1A8, targeting the Marburg glycoprotein, did not interfere with the binding either, and the 5.13% of double-positive may be due to the nonspecific-binding of 1A8 to S protein. 4A8 also failed to interfere with the binding of the S protein to ACE2.

Cryo-EM structure of the complex between 4A8 and S-ECD

The mAb 4A8 was overexpressed and purified by Protein A resin and the S-ECD of SARS-CoV-2 was purified through M2 affinity resin and size exclusion chromatography (SEC). 4A8 and S-ECD protein were mixed and incubated at a stoichiometric ratio of ~ 1.2 to 1 for 1 hour and applied to SEC to remove excess proteins (fig. S3A). The fraction containing the complex was concentrated for cryo-EM sample preparation.

To investigate the interactions between 4A8 and the S protein, we solved the cryo-EM structure of the complex at an overall resolution of 3.1 Å (Fig. 5 and movie S1). Details of cryo-EM sample preparation, data collection and processing, and model building can be found in Materials and Methods section in supplementary materials (figs. S3 to S5). The S protein exhibits asymmetric conformations similar to the previously reported structures (*21*, *22*), with one of three RBDs in "up" conformation and the other two RBDs in "down" conformation (Fig. 5).

Recognition of the NTD by 4A8

In the S protein-4A8 complex, each trimeric S protein is bound with three solved 4A8 Fabs, each of which interacts with one NTD of the S protein. Despite the different conformations of the three S protein protomers, the interface between 4A8 and each NTD is identical (Fig. 5 and fig. S3I). The map quality at the NTD-4A8 region was improved by focused refinement to a local resolution of 3.3 Å, enabling reliable analysis of the interactions between the NTD and 4A8.

Association with 4A8 appears to stabilize the NTD epitope, which is invisible in the reported S protein structure alone (*21*, *22*). Supported by the high resolution of NTD, we were able to build the structural model for five new loops for NTD, designated N1 (residues 14-26), N2 (residues 67-79), N3 (residues 141-156), N4 (residues 177-186) and N5 (residues 246-260), among which the N3 and N5 loops mediate the interaction with 4A8 (fig. S5A). Besides, three new glycosylation sites (Asn17, Asn61, Asn149) on the NTD are identified in this structure (fig. S6).

The heavy chain of 4A8 mainly participates in binding to the NTD mainly through three complementarity-determining regions (CDRs), named CDR1 (residues 25-32), CDR2 (residues 51-58) and CDR3 (residues 100-116) (Fig. 6A and fig. S5B). The interface is constituted by an extensive hydrophilic

interaction network and the buried surface area at the 4A8-NTD interface is 832 Å^2. Arg246 on the N5 loop of the NTD represents one docking site, which is stabilized by Trp258, simultaneously interacting with Tyr27 and Glu31 of 4A8 on CDR1 (Fig. 6B). On the N3 loop of the NTD, Lys150 and Lys147 respectively form salt bridges with Glu54 and Glu72 of 4A8 (Fig. 6C). Lys150 is also hydrogen bonded (H-bond) with 4A8-Tyr111, while His146 forms a H-bond with 4A8-Thr30 (Fig. 6C). In addition to the hydrophilic interactions, Trp152 and Tyr145 on the N3 loop of the NTD also interact with Val102, Pro106, and Phe109 on the CDR3 of 4A8 through hydrophobic and/or π-π interactions (Fig. 6D). Besides, the glycosylation site of Asn149 on the NTD is close to the 4A8-NTD interface, of which N-glycans might participate in the interactions on the interface (Fig. 6A and fig. S6).

Discussion

There is an urgent need for prophylactic and therapeutic interventions for SARS-CoV-2 infections given the ongoing COVID-19 pandemic. Our work reveals that naturally occurring human SARS-CoV-2 mAbs isolated from the B cells of 10 recovered donors are diverse in gene usage and epitope recognition of S protein. Remarkably, the majority of the isolated mAbs did not recognize the RBD, and all the mAbs that neutralize authentic SARS-CoV-2 failed to inhibit the binding of S protein to ACE2. These unexpected results suggest the presence of other important mechanisms for SARS-CoV-2 neutralization in addition to suppressing the viral interaction with the receptor.

The S1-targeting mAb 4A8 does not block the interaction between ACE2 and S protein, but exhibits high levels of neutralization against both authentic and pseudotyped SARS-CoV-2 in vitro. Many neutralizing antibodies against the SARS-CoV-2 were reported to target the RBD of the S protein and block the binding between RBD and ACE2 (*28–30*, *32–34*). Our results show that 4A8 binds to the NTD of S protein with potent neutralizing activity. Previous study showed that mAb 7D10 could bind to the NTD of S protein of MERS-CoV probably by inhibiting the RBD-DPP4 binding and the prefusion to postfusion conformational change of S protein (*26*). We aligned the crystal structure of 7D10 in complex with the NTD of S protein of MERS-CoV with our complex structure and found that the interfaces between the mAb and the NTDs are partially overlapped (fig. S7). 7D10 may inhibit the interaction between MERS-CoV and DPP4 through its light chain that is close to the RBD. In our complex, the light chain of 4A8 is away from the RBD (fig. S7). Therefore, we speculate that 4A8 may neutralize SARS-CoV-2 by restraining the conformational changes of the S protein. Furthermore, sequences alignment of the S proteins from SARS-CoV-2, SARS-CoV, and MERS-CoV revealed varied NTD surface sequences that are respectively recognized by different mAbs (fig. S8).

Overall, this work reports a fully human neutralizing mAb recognizing a vulnerable epitope of NTD on S protein of SARS-CoV-2, functioning with a mechanism that is independent of receptor binding inhibition. Combination of 4A8 with RBD-targeting antibodies may avoid the escaping mutations of virus and serve as promising "cocktail" therapeutics. The information obtained from these studies can be used for development of the structure-based vaccine design against SARS-CoV-2.

REFERENCES AND NOTES

1. N. Zhu, D. Zhang, W. Wang, X. Li, B. Yang, J. Song, X. Zhao, B. Huang, W. Shi, R. Lu, P. Niu, F. Zhan, X. Ma, D. Wang, W. Xu, G. Wu, G. F. Gao, W. Tan; China Novel Coronavirus Investigating and Research Team, A Novel Coronavirus from Patients with Pneumonia in China, 2019. *N. Engl. J. Med.* **382**, 727–733 (2020). doi:10.1056/NEJMoa2001017 Medline
2. F. Wu, S. Zhao, B. Yu, Y.-M. Chen, W. Wang, Z.-G. Song, Y. Hu, Z.-W. Tao, J.-H. Tian, Y.-Y. Pei, M.-L. Yuan, Y.-L. Zhang, F.-H. Dai, Y. Liu, Q.-M. Wang, J.-J. Zheng, L. Xu, E. C. Holmes, Y.-Z. Zhang, A new coronavirus associated with human respiratory disease in China. *Nature* **579**, 265–269 (2020). doi:10.1038/s41586-020-2008-3 Medline
3. C. Huang, Y. Wang, X. Li, L. Ren, J. Zhao, Y. Hu, L. Zhang, G. Fan, J. Xu, X. Gu, Z. Cheng, T. Yu, J. Xia, Y. Wei, W. Wu, X. Xie, W. Yin, H. Li, M. Liu, Y. Xiao, H. Gao, L. Guo, J. Xie, G. Wang, R. Jiang, Z. Gao, Q. Jin, J. Wang, B. Cao, Clinical features of patients infected with 2019 novel coronavirus in Wuhan, China. *Lancet* **395**, 497–506 (2020). doi:10.1016/S0140-6736(20)30183-5 Medline
4. P. Zhou, X.-L. Yang, X.-G. Wang, B. Hu, L. Zhang, W. Zhang, H.-R. Si, Y. Zhu, B. Li, C.-L. Huang, H.-D. Chen, J. Chen, Y. Luo, H. Guo, R.-D. Jiang, M.-Q. Liu, Y. Chen, X.-R. Shen, X. Wang, X.-S. Zheng, K. Zhao, Q.-J. Chen, F. Deng, L.-L. Liu, B. Yan, F.-X. Zhan, Y.-Y. Wang, G.-F. Xiao, Z.-L. Shi, A pneumonia outbreak associated with a new coronavirus of probable bat origin. *Nature* **579**, 270–273 (2020). doi:10.1038/s41586-020-2012-7 Medline
5. C. C. Lai, T. P. Shih, W. C. Ko, H. J. Tang, P. R. Hsueh, Severe acute respiratory syndrome coronavirus 2 (SARS-CoV-2) and coronavirus disease-2019 (COVID-19): The epidemic and the challenges. *Int. J. Antimicrob. Agents* **55**, 105924 (2020). doi:10.1016/j.ijantimicag.2020.105924 Medline
6. T. G. Ksiazek, D. Erdman, C. S. Goldsmith, S. R. Zaki, T. Peret, S. Emery, S. Tong, C. Urbani, J. A. Comer, W. Lim, P. E. Rollin, S. F. Dowell, A.-E. Ling, C. D. Humphrey, W.-J. Shieh, J. Guarner, C. D. Paddock, P. Rota, B. Fields, J. DeRisi, J.-Y. Yang, N. Cox, J. M. Hughes, J. W. LeDuc, W. J. Bellini, L. J. Anderson; SARS Working Group, A novel coronavirus associated with severe acute respiratory syndrome. *N. Engl. J. Med.* **348**, 1953–1966 (2003). doi:10.1056/NEJMoa030781 Medline
7. A. M. Zaki, S. van Boheemen, T. M. Bestebroer, A. D. Osterhaus, R. A. Fouchier, Isolation of a novel coronavirus from a man with pneumonia in Saudi Arabia. *N. Engl. J. Med.* **367**, 1814–1820 (2012). doi:10.1056/NEJMoa1211721 Medline
8. W. Li, M. J. Moore, N. Vasilieva, J. Sui, S. K. Wong, M. A. Berne, M. Somasundaran, J. L. Sullivan, K. Luzuriaga, T. C. Greenough, H. Choe, M. Farzan, Angiotensin-converting enzyme 2 is a functional receptor for the SARS coronavirus. *Nature* **426**, 450–454 (2003). doi:10.1038/nature02145 Medline
9. J. H. Kuhn, W. Li, H. Choe, M. Farzan, Angiotensin-converting enzyme 2: A functional receptor for SARS coronavirus. *Cell. Mol. Life Sci.* **61**, 2738–2743 (2004). doi:10.1007/s00018-004-4242-5 Medline
10. K. Kuba, Y. Imai, S. Rao, H. Gao, F. Guo, B. Guan, Y. Huan, P. Yang, Y. Zhang, W. Deng, L. Bao, B. Zhang, G. Liu, Z. Wang, M. Chappell, Y. Liu, D. Zheng, A. Leibbrandt, T. Wada, A. S. Slutsky, D. Liu, C. Qin, C. Jiang, J. M. Penninger, A crucial role of angiotensin converting enzyme 2 (ACE2) in SARS coronavirus-induced lung injury. *Nat. Med.* **11**, 875–879 (2005). doi:10.1038/nm1267 Medline
11. D. S. Dimitrov, The secret life of ACE2 as a receptor for the SARS virus. *Cell* **115**, 652–653 (2003). doi:10.1016/S0092-8674(03)00976-0 Medline
12. J. Lan, J. Ge, J. Yu, S. Shan, H. Zhou, S. Fan, Q. Zhang, X. Shi, Q. Wang, L. Zhang, X. Wang, Structure of the SARS-CoV-2 spike receptor-binding domain bound to the ACE2 receptor. *Nature* **581**, 215–220 (2020). doi:10.1038/s41586-020-2180-5 Medline

13. Q. Wang, Y. Zhang, L. Wu, S. Niu, C. Song, Z. Zhang, G. Lu, C. Qiao, Y. Hu, K.-Y. Yuen, Q. Wang, H. Zhou, J. Yan, J. Qi, Structural and functional basis of SARS-CoV-2 entry by using human ACE2. *Cell* **181**, 894–904.e9 (2020). doi:10.1016/j.cell.2020.03.045 Medline
14. R. Yan, Y. Zhang, Y. Li, L. Xia, Y. Guo, Q. Zhou, Structural basis for the recognition of SARS-CoV-2 by full-length human ACE2. *Science* **367**, 1444–1448 (2020). doi:10.1126/science.abb2762 Medline
15. J. Shang, G. Ye, K. Shi, Y. Wan, C. Luo, H. Aihara, Q. Geng, A. Auerbach, F. Li, Structural basis of receptor recognition by SARS-CoV-2. *Nature* **581**, 221–224 (2020). doi:10.1038/s41586-020-2179-y Medline
16. M. Hoffmann, H. Kleine-Weber, S. Schroeder, N. Krüger, T. Herrler, S. Erichsen, T. S. Schiergens, G. Herrler, N.-H. Wu, A. Nitsche, M. A. Müller, C. Drosten, S. Pöhlmann, SARS-CoV-2 cell entry depends on ACE2 and TMPRSS2 and is blocked by a clinically proven protease inhibitor. *Cell* **181**, 271–280.e8 (2020). doi:10.1016/j.cell.2020.02.052 Medline
17. T. M. Gallagher, M. J. Buchmeier, Coronavirus spike proteins in viral entry and pathogenesis. *Virology* **279**, 371–374 (2001). doi:10.1006/viro.2000.0757 Medline
18. G. Simmons, P. Zmora, S. Gierer, A. Heurich, S. Pöhlmann, Proteolytic activation of the SARS-coronavirus spike protein: Cutting enzymes at the cutting edge of antiviral research. *Antiviral Res.* **100**, 605–614 (2013). doi:10.1016/j.antiviral.2013.09.028 Medline
19. S. Belouzard, V. C. Chu, G. R. Whittaker, Activation of the SARS coronavirus spike protein via sequential proteolytic cleavage at two distinct sites. *Proc. Natl. Acad. Sci. U.S.A.* **106**, 5871–5876 (2009). doi:10.1073/pnas.0809524106 Medline
20. W. Song, M. Gui, X. Wang, Y. Xiang, Cryo-EM structure of the SARS coronavirus spike glycoprotein in complex with its host cell receptor ACE2. *PLOS Pathog.* **14**, e1007236 (2018). doi:10.1371/journal.ppat.1007236 Medline
21. D. Wrapp, N. Wang, K. S. Corbett, J. A. Goldsmith, C.-L. Hsieh, O. Abiona, B. S. Graham, J. S. McLellan, Cryo-EM structure of the 2019-nCoV spike in the prefusion conformation. *Science* **367**, 1260–1263 (2020). doi:10.1126/science.abb2507 Medline
22. A. C. Walls, Y.-J. Park, M. A. Tortorici, A. Wall, A. T. McGuire, D. Veesler, Structure, Function, and Antigenicity of the SARS-CoV-2 Spike Glycoprotein. *Cell* **181**, 281–292.e6 (2020). doi:10.1016/j.cell.2020.02.058 Medline
23. C. Krempl, B. Schultze, H. Laude, G. Herrler, Point mutations in the S protein connect the sialic acid binding activity with the enteropathogenicity of transmissible gastroenteritis coronavirus. *J. Virol.* **71**, 3285–3287 (1997). doi:10.1128/JVI.71.4.3285-3287.1997 Medline
24. F. Künkel, G. Herrler, Structural and functional analysis of the surface protein of human coronavirus OC43. *Virology* **195**, 195–202 (1993). doi:10.1006/viro.1993.1360 Medline
25. G. Lu, Q. Wang, G. F. Gao, Bat-to-human: Spike features determining 'host jump' of coronaviruses SARS-CoV, MERS-CoV, and beyond. *Trends Microbiol.* **23**, 468–478 (2015). doi:10.1016/j.tim.2015.06.003 Medline
26. H. Zhou, Y. Chen, S. Zhang, P. Niu, K. Qin, W. Jia, B. Huang, S. Zhang, J. Lan, L. Zhang, W. Tan, X. Wang, Structural definition of a neutralization epitope on the N-terminal domain of MERS-CoV spike glycoprotein. *Nat. Commun.* **10**, 3068 (2019). doi:10.1038/s41467-019-10897-4 Medline
27. B. Ju *et al.*, Potent human neutralizing antibodies elicited by SARS-CoV-2 infection. *bioRxiv* 2020.03.21.990770 (2020).
28. C. Wang, W. Li, D. Drabek, N. M. A. Okba, R. van Haperen, A. D. M. E. Osterhaus, F. J. M. van Kuppeveld, B. L. Haagmans, F. Grosveld, B.-J. Bosch, A human monoclonal antibody blocking SARS-CoV-2 infection. *Nat. Commun.* **11**, 2251 (2020). doi:10.1038/s41467-020-16256-y Medline
29. D. Wrapp, D. De Vlieger, K. S. Corbett, G. M. Torres, N. Wang, W. Van Breedam, K. Roose, L. van Schie, M. Hoffmann, S. Pöhlmann, B. S. Graham, N. Callewaert, B. Schepens, X. Saelens, J. S. McLellan; VIB-CMB COVID-19 Response Team, Structural Basis for Potent Neutralization of Betacoronaviruses by Single-Domain Camelid Antibodies. *Cell* **181**, 1004–1015.e15 (2020). doi:10.1016/j.cell.2020.04.031 Medline
30. X. Chen, R. Li, Z. Pan, C. Qian, Y. Yang, R. You, J. Zhao, P. Liu, L. Gao, Z. Li, Q. Huang, L. Xu, J. Tang, Q. Tian, W. Yao, L. Hu, X. Yan, X. Zhou, Y. Wu, K. Deng, Z. Zhang, Z. Qian, Y. Chen, L. Ye, Human monoclonal antibodies block the binding of SARS-CoV-2 spike protein to angiotensin converting enzyme 2 receptor. *Cell. Mol. Immunol.* **17**, 647–649 (2020). doi:10.1038/s41423-020-0426-7 Medline
31. M. Yuan, N. C. Wu, X. Zhu, C. D. Lee, R. T. Y. So, H. Lv, C. K. P. Mok, I. A. Wilson, A highly conserved cryptic epitope in the receptor binding domains of SARS-CoV-2 and SARS-CoV. *Science* **368**, 630–633 (2020). doi:10.1126/science.abb7269 Medline
32. Y. Wu, F. Wang, C. Shen, W. Peng, D. Li, C. Zhao, Z. Li, S. Li, Y. Bi, Y. Yang, Y. Gong, H. Xiao, Z. Fan, S. Tan, G. Wu, W. Tan, X. Lu, C. Fan, Q. Wang, Y. Liu, C. Zhang, J. Qi, G. F. Gao, F. Gao, L. Liu, A noncompeting pair of human neutralizing antibodies block COVID-19 virus binding to its receptor ACE2. *Science* **368**, 1274–1278 (2020). doi:10.1126/science.abc2241 Medline
33. B. Ju, Q. Zhang, J. Ge, R. Wang, J. Sun, X. Ge, J. Yu, S. Shan, B. Zhou, S. Song, X. Tang, J. Yu, J. Lan, J. Yuan, H. Wang, J. Zhao, S. Zhang, Y. Wang, X. Shi, L. Liu, J. Zhao, X. Wang, Z. Zhang, L. Zhang, Human neutralizing antibodies elicited by SARS-CoV-2 infection. *Nature* (2020). doi:10.1038/s41586-020-2380-z Medline
34. Y. Cao, B. Su, X. Guo, W. Sun, Y. Deng, L. Bao, Q. Zhu, X. Zhang, Y. Zheng, C. Geng, X. Chai, R. He, X. Li, Q. Lv, H. Zhu, W. Deng, Y. Xu, Y. Wang, L. Qiao, Y. Tan, L. Song, G. Wang, X. Du, N. Gao, J. Liu, J. Xiao, X. D. Su, Z. Du, Y. Feng, C. Qin, C. Qin, R. Jin, X. S. Xie, Potent neutralizing antibodies against SARS-CoV-2 identified by high-throughput single-cell sequencing of convalescent patients' B cells. *Cell* (2020). doi:10.1016/j.cell.2020.05.025 Medline
35. A. Burkovitz, I. Sela-Culang, Y. Ofran, Large-scale analysis of somatic hypermutations in antibodies reveals which structural regions, positions and amino acids are modified to improve affinity. *FEBS J.* **281**, 306–319 (2014). doi:10.1111/febs.12597 Medline
36. E. P. Rock, P. R. Sibbald, M. M. Davis, Y. H. Chien, CDR3 length in antigen-specific immune receptors. *J. Exp. Med.* **179**, 323–328 (1994). doi:10.1084/jem.179.1.323 Medline
37. C. G. Price, P. W. Abrahams, Copper tolerance in a population of Silene vulgaris ssp. maritima (A. & D. Love) at Dolfrwynog Bog near Dolgellau, North Wales. *Environ. Geochem. Health* **16**, 27–30 (1994). doi:10.1007/BF00149590 Medline
38. S. Kumar, G. Stecher, K. Tamura, MEGA7: Molecular Evolutionary Genetics Analysis Version 7.0 for Bigger Datasets. *Mol. Biol. Evol.* **33**, 1870–1874 (2016). doi:10.1093/molbev/msw054 Medline
39. Q. Li, Q. Liu, W. Huang, J. Wu, J. Nie, M. Wang, C. Zhao, L. Zhang, Y. Wang, An LASV GPC pseudotyped virus based reporter system enables evaluation of vaccines in mice under non-BSL-4 conditions. *Vaccine* **35**, 5172–5178 (2017). doi:10.1016/j.vaccine.2017.07.101 Medline
40. J. Xu, W. Jia, P. Wang, S. Zhang, X. Shi, X. Wang, L. Zhang, Antibodies and vaccines against Middle East respiratory syndrome coronavirus. *Emerg. Microbes Infect.* **8**, 841–856 (2019). doi:10.1080/22221751.2019.1624482 Medline
41. L. Wang, W. Shi, J. D. Chappell, M. G. Joyce, Y. Zhang, M. Kanekiyo, M. M. Becker, N. van Doremalen, R. Fischer, N. Wang, K. S. Corbett, M. Choe, R. D. Mason, J. G. Van Galen, T. Zhou, K. O. Saunders, K. M. Tatti, L. M. Haynes, P. D. Kwong, K. Modjarrad, W.-P. Kong, J. S. McLellan, M. R. Denison, V. J. Munster, J. R. Mascola, B. S. Graham, Importance of neutralizing monoclonal antibodies targeting multiple antigenic sites on the middle east respiratory syndrome coronavirus spike glycoprotein to avoid neutralization escape. *J. Virol.* **92**, e02002-17 (2018). doi:10.1128/JVI.02002-17 Medline
42. J. Shang, Y. Wan, C. Luo, G. Ye, Q. Geng, A. Auerbach, F. Li, Cell entry mechanisms of SARS-CoV-2. *Proc. Natl. Acad. Sci. U.S.A.* **117**, 11727–11734 (2020). doi:10.1073/pnas.2003138117 Medline
43. K. Smith, L. Garman, J. Wrammert, N.-Y. Zheng, J. D. Capra, R. Ahmed, P. C. Wilson, Rapid generation of fully human monoclonal antibodies specific to a vaccinating antigen. *Nat. Protoc.* **4**, 372–384 (2009). doi:10.1038/nprot.2009.3 Medline
44. H. X. Liao, M. C. Levesque, A. Nagel, A. Dixon, R. Zhang, E. Walter, R. Parks, J. Whitesides, D. J. Marshall, K.-K. Hwang, Y. Yang, X. Chen, F. Gao, S. Munshaw, T. B. Kepler, T. Denny, M. A. Moody, B. F. Haynes, High-throughput isolation of immunoglobulin genes from single human B cells and expression as monoclonal antibodies. *J. Virol. Methods* **158**, 171–179 (2009). doi:10.1016/j.jviromet.2009.02.014 Medline

45. J. Ye, N. Ma, T. L. Madden, J. M. Ostell, IgBLAST: An immunoglobulin variable domain sequence analysis tool. *Nucleic Acids Res.* **41**, W34-40 (2013). doi:10.1093/nar/gkt382 Medline
46. V. Giudicelli, X. Brochet, M. P. Lefranc, IMGT/V-QUEST: IMGT standardized analysis of the immunoglobulin (IG) and T cell receptor (TR) nucleotide sequences. *Cold Spring Harb. Protoc.* **2011**, 695–715 (2011). doi:10.1101/pdb.prot5633 Medline
47. N. T. Gupta, J. A. Vander Heiden, M. Uduman, D. Gadala-Maria, G. Yaari, S. H. Kleinstein, Change-O: A toolkit for analyzing large-scale B cell immunoglobulin repertoire sequencing data. *Bioinformatics* **31**, 3356–3358 (2015). doi:10.1093/bioinformatics/btv359 Medline
48. N. Saitou, M. Nei, The neighbor-joining method: A new method for reconstructing phylogenetic trees. *Mol. Biol. Evol.* **4**, 406–425 (1987). Medline
49. J. Felsenstein, Confidence limits on phylogenies: An approach using the bootstrap. *Evolution* **39**, 783–791 (1985). doi:10.1111/j.1558-5646.1985.tb00420.x Medline
50. K. Tamura, M. Nei, S. Kumar, Prospects for inferring very large phylogenies by using the neighbor-joining method. *Proc. Natl. Acad. Sci. U.S.A.* **101**, 11030–11035 (2004). doi:10.1073/pnas.0404206101 Medline
51. J. D. Thompson, T. J. Gibson, D. G. Higgins, Multiple sequence alignment using ClustalW and ClustalX. *Curr Protoc Bioinformatics* **Chapter 2**, Unit 2.3 (2002).
52. W. J. Wilbur, D. J. Lipman, Rapid similarity searches of nucleic acid and protein data banks. *Proc. Natl. Acad. Sci. U.S.A.* **80**, 726–730 (1983). doi:10.1073/pnas.80.3.726 Medline
53. J. Lei, J. Frank, Automated acquisition of cryo-electron micrographs for single particle reconstruction on an FEI Tecnai electron microscope. *J. Struct. Biol.* **150**, 69–80 (2005). doi:10.1016/j.jsb.2005.01.002 Medline
54. S. Q. Zheng, E. Palovcak, J.-P. Armache, K. A. Verba, Y. Cheng, D. A. Agard, MotionCor2: Anisotropic correction of beam-induced motion for improved cryo-electron microscopy. *Nat. Methods* **14**, 331–332 (2017). doi:10.1038/nmeth.4193 Medline
55. T. Grant, N. Grigorieff, Measuring the optimal exposure for single particle cryo-EM using a 2.6 Å reconstruction of rotavirus VP6. *eLife* **4**, e06980 (2015). doi:10.7554/eLife.06980 Medline
56. K. Zhang, Gctf: Real-time CTF determination and correction. *J. Struct. Biol.* **193**, 1–12 (2016). doi:10.1016/j.jsb.2015.11.003 Medline
57. J. Zivanov, T. Nakane, B. O. Forsberg, D. Kimanius, W. J. H. Hagen, E. Lindahl, S. H. W. Scheres, New tools for automated high-resolution cryo-EM structure determination in RELION-3. *eLife* **7**, e42166 (2018). doi:10.7554/eLife.42166 Medline
58. D. Kimanius, B. O. Forsberg, S. H. Scheres, E. Lindahl, Accelerated cryo-EM structure determination with parallelisation using GPUs in RELION-2. *eLife* **5**, e18722 (2016). doi:10.7554/eLife.18722 Medline
59. S. H. Scheres, RELION: Implementation of a Bayesian approach to cryo-EM structure determination. *J. Struct. Biol.* **180**, 519–530 (2012). doi:10.1016/j.jsb.2012.09.006 Medline
60. S. H. Scheres, A Bayesian view on cryo-EM structure determination. *J. Mol. Biol.* **415**, 406–418 (2012). doi:10.1016/j.jmb.2011.11.010 Medline
61. A. Punjani, J. L. Rubinstein, D. J. Fleet, M. A. Brubaker, cryoSPARC: Algorithms for rapid unsupervised cryo-EM structure determination. *Nat. Methods* **14**, 290–296 (2017). doi:10.1038/nmeth.4169 Medline
62. P. B. Rosenthal, R. Henderson, Optimal determination of particle orientation, absolute hand, and contrast loss in single-particle electron cryomicroscopy. *J. Mol. Biol.* **333**, 721–745 (2003). doi:10.1016/j.jmb.2003.07.013 Medline
63. S. Chen, G. McMullan, A. R. Faruqi, G. N. Murshudov, J. M. Short, S. H. W. Scheres, R. Henderson, High-resolution noise substitution to measure overfitting and validate resolution in 3D structure determination by single particle electron cryomicroscopy. *Ultramicroscopy* **135**, 24–35 (2013). doi:10.1016/j.ultramic.2013.06.004 Medline
64. L. G. Trabuco, E. Villa, K. Mitra, J. Frank, K. Schulten, Flexible fitting of atomic structures into electron microscopy maps using molecular dynamics. *Structure* **16**, 673–683 (2008). doi:10.1016/j.str.2008.03.005 Medline
65. P. Emsley, B. Lohkamp, W. G. Scott, K. Cowtan, Features and development of Coot. *Acta Crystallogr. D Biol. Crystallogr.* **66**, 486–501 (2010). doi:10.1107/S0907444910007493 Medline
66. P. D. Adams, P. V. Afonine, G. Bunkóczi, V. B. Chen, I. W. Davis, N. Echols, J. J. Headd, L.-W. Hung, G. J. Kapral, R. W. Grosse-Kunstleve, A. J. McCoy, N. W. Moriarty, R. Oeffner, R. J. Read, D. C. Richardson, J. S. Richardson, T. C. Terwilliger, P. H. Zwart, PHENIX: A comprehensive Python-based system for macromolecular structure solution. *Acta Crystallogr. D Biol. Crystallogr.* **66**, 213–221 (2010). doi:10.1107/S0907444909052925 Medline

ACKNOWLEDGMENTS

We thank the Cryo-EM Facility and Supercomputer Center of Westlake University for providing cryo-EM and computation support, respectively. We thank the Beijing Institute of Microbiology and Epidemiology, Academy of Military Medical Sciences, China, for providing the SARS-CoV-2. We also thank Ting Fang, Ting Yu, Peng Lv, and Enhao Ma for providing technical support. **Funding:** This work was funded by the National Key R&D Program of China (2020YFC0841400), the National Natural Science Foundation of China (projects 31971123, 81803429, 81703048, 31900671, 81920108015, 31930059), the Key R&D Program of Zhejiang Province (2020C04001), the SARS-CoV-2 emergency project of the Science and Technology Department of Zhejiang Province (2020C03129), the Leading Innovative and Entrepreneur Team Introduction Program of Hangzhou, the National Science and Technology Major Project of the Ministry of Science and Technology of China, (2018ZX10101003-005-007), and Special Research Program of Novel Coronavirus Pneumonia of Westlake University. **Author contributions:** W.C., Q.Z. and J.L. conceived the project. X.C., R.Y., J.Z., G.Z., Y.Z., Y.G., Y.L., L.X., M.H., Z.Z., P.F., Y.D., Z.C., J.L.Z., X.S., Y.C., L.F., L.H., J.X. and C.Y. did the experiments. All authors contributed to data analysis. X.C., R.Y., J.L., Q.Z. and W.C. wrote the manuscript. **Competing interests:** W.C., J.L., X.C., J.Z., L.F., C.Y., J.X., L.H., G.Z., P.F., M.H., Y.D., X.S., Y.C., and J.Z. are listed as inventors on a pending patent application for mAb 4A8. The other authors declare that they have no competing interests. **Data and materials availability:** Atomic coordinates and cryo EM density maps of the S protein of SARS-CoV-2 in complex bound with 4A8 (PDB: 7C2L; whole map: EMD-30276, antibody-epitope interface-focused refined map: EMD-30277) have been deposited to the Protein Data Bank (http://www.rcsb.org) and the Electron Microscopy Data Bank (https://www.ebi.ac.uk/pdbe/emdb), respectively. Antibody sequences have been deposited at GenBank (MTA 622682 – 622751).

SUPPLEMENTARY MATERIALS

science.sciencemag.org/cgi/content/full/science.abc6952/DC1
Materials and Methods
Figs. S1 to S7
Tables S1 to S4
References (*43–66*)
Movie S1
MDAR Reproducibility Checklist

8 May 2020; accepted 17 June 2020
Published online 22 June 2020
10.1126/science.abc6952

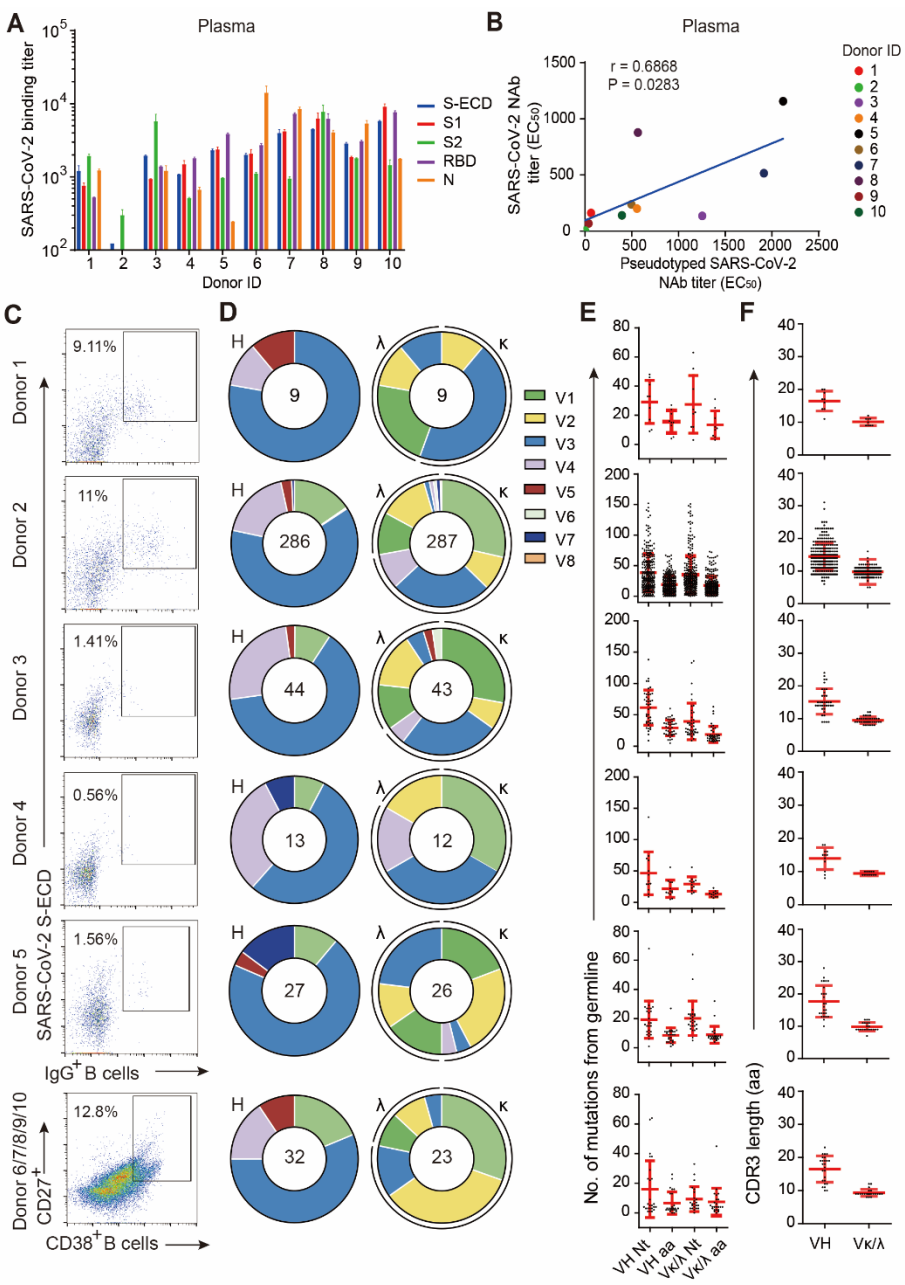

Fig. 1. Isolation of antigen-specific monoclonal antibodies from convalescent patients of SARS-CoV-2. (**A**) Reactions of plasma to SARS-CoV-2 proteins. S-ECD (extracellular domain of S protein), S1, S2, RBD (receptor binding domain) and N (nucleocapsid protein) were used in ELISA to test the binding of plasma. Plasma of heathy donors were used as control, and cut-off values were calculated as O.D. 450 of control × 2.1. Data were shown with mean and SD of a representative experiment. (**B**) The correlations between the authentic SARS-CoV-2 neutralizing antibody (NAb) titers and the pseudotyped SARS-CoV-2 neutralizing antibody titers in plasma. Neutralizing assays of plasma against authentic SARS-CoV-2 were performed using Vero E6 cells, and neutralization against pseudotyped SARS-CoV-2 were determined using ACE2-293T cells. The correlations were calculated by Pearson correlation test in Graphpad 7.0. (**C**) Flow cytometry sorting from PBMCs of 10 convalescent patients. (**D**) Distribution of V gene families in heavy and light chains of all unique clones (the total number is shown in the center of the pie charts) for each donor. (**E**) The Number of amino acid (AA) and total nucleotide (Nt) mutations from the germline of all clonal sequences identified in (D) was shown. (**F**) CDR3 amino acid lengths of VH and VL of all clonal sequences identified in (D).

A ELISA binding (EC_{50}: ng/mL)

Group	Donor	mAb	S-ECD	S1	RBD	S2
1	3	0304-2F8	1883	>	>	>
	5	0317-A3	3025	>	>	>
	5	0317-A9	5851	>	>	>
	5	0317-B1	9470	>	>	>
	5	0317-C4	7624	>	>	>
	6/7/8/9/10	10C10	78	>	>	>
2A	4	0304-4A2	5	3	>	>
	5	0317-A7	9	6	>	>
	5	0317-A8	1702	1812	>	>
	6/7/8/9/10	4A8	5	8	>	>
2B	1	1M-1D2	17	125	519	>
	2	2M-10B11	8	4	5	>
	2	2M-4G4	9102	>	164	>
3A	2	2M-14B2	1479	1700	1075	210
3B	2	2M-2D4	2138	9250	>	749
	2	2M-2G12	5715	7973	>	4838
	2	2M-7E9	183	7899	>	86
	2	2M-8E7	189	9783	>	70
	4	0304-3H3	5	2094	>	3
	4	0304-4A10	3	3875	>	3
	5	0317-A1	119	4697	>	139
4	2	2M-2D1	7177	>	>	1233
	2	2M-8H10	37	>	>	23
	2	2M-9F10	2959	>	>	863
	2	2M-9H1	77	>	>	19
	2	2M-12D7	42	>	>	13
	2	2M-13A3	107	>	>	24
	2	2M-13D11	137	>	>	9
	2	2M-14E4	33	>	>	9
	2	2M-14E5	11	>	>	7
	5	0317-A2	1460	>	>	2080
	5	0317-C9	7965	>	>	6429
	6/7/8/9/10	8D2	49	>	>	5489
	6/7/8/9/10	8D9	2678	>	>	642
	6/7/8/9/10	9A1	16	>	>	5

B

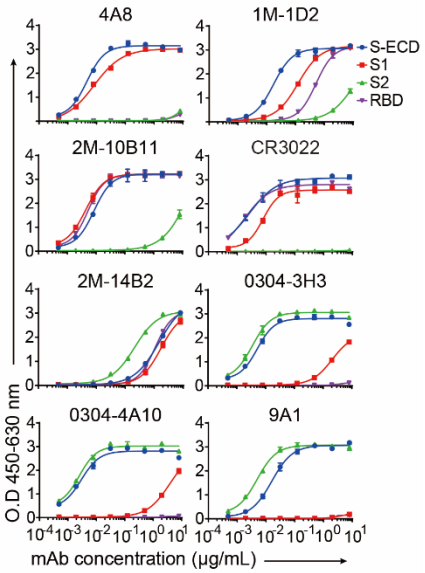

C Detecting Antibody

Blocking Antibody: Group	mAb	2A 0304-4A2	2A 4A8	2B 1M-1D2	2B 2M-10B11	CR 3022	3B 0304-4A10	4 2M-14E4	4 9A1	4 2M-13D11	4 2M-13A3	4 2M-14E5
2A	0304-4A2	3	127	111	108	104	106	135	114	110	135	128
	4A8	90	4	6	107	102	103	147	111	96	132	130
2B	1M-1D2	88	93	5	107	98	102	128	106	76	119	128
	2M-10B11	84	95	128	6	13	92	123	103	75	110	99
	CR 3022	98	131	115	57	8	104	128	111	116	230	167
3B	0304-4A10	94	110	111	102	106	7	16	112	96	224	179
4	2M-14E4	76	102	119	101	101	91	12	116	86	165	107
	9A1	87	90	119	102	98	102	116	6	6	117	120
	2M-13D11	83	112	110	104	104	104	179	105	6	57	85
	2M-13A3	104	112	114	105	102	104	256	109	62	13	28
	2M-14E5	79	103	110	101	98	105	134	113	84	14	7

D

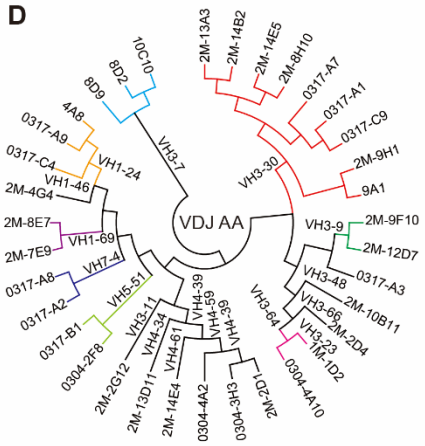

Fig. 2. Binding profiles of Spike protein-specific mAbs. (**A**) Heatmap showing the binding of mAbs to different types of spike proteins determined using ELISA. The EC_{50} value for each S-mAb combination is shown, with dark red, orange, yellow, or white shading indicating high, intermediate, low, or no detectable binding, respectively. EC_{50} values greater than 10,000 ng/ml are indicated (>). (**B**) Binding curves of representative mAbs. CR3022 is a control that was reported to bind SARS-CoV and SARS-CoV-2 RBD. Data were shown with mean and SD of a representative experiment. (**C**) Heatmap showing the competing binding of some representative S-reactive mAbs assayed in ELISA. Numbers in the box indicate the percentage binding of detecting mAb in the presence of the blocking antibody compared to the binding of detecting mAb in the absence of the blocking antibody. The mAbs were considered competing if the inhibiting percentage is <30% (black boxes with white numbers). The mAbs were judged to non-compete for the same site if the percentage is >70% (white boxes with red numbers. Gray boxes with black numbers indicate an intermediate phenotype (30%~70%). (**D**) Phylogenetic trees of all the S-specific mAbs.

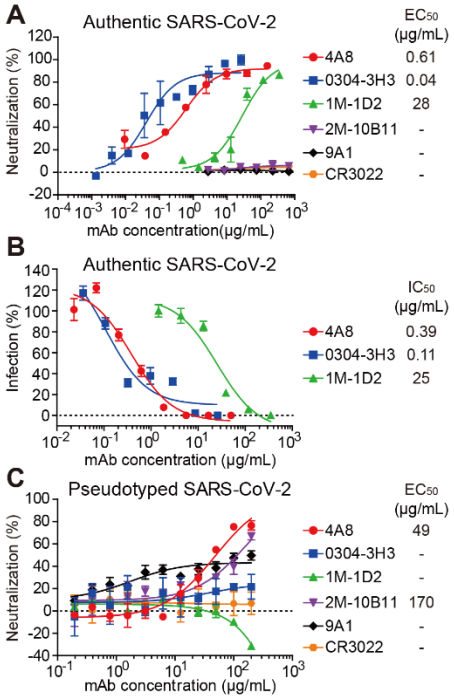

Fig. 3. Neutralizing capacities of S-reactive mAbs. (**A**) Neutralization of S-reactive mAbs to authentic SARS-CoV-2 in Vero-E6 cells. (**B**) The authentic SARS-CoV-2 virus RNA load was determined in Vero-E6 cells treated with S-reactive mAbs using qPCR. Percent infection was calculated as the ratio of RNA load in mAb-treated wells to that in wells containing virus only. (**C**) Neutralization of S-reactive mAbs against HIV-vectored pseudotyped SARS-CoV-2 in ACE2-293T cells. Data were shown as mean ± SD of a representative experiment.

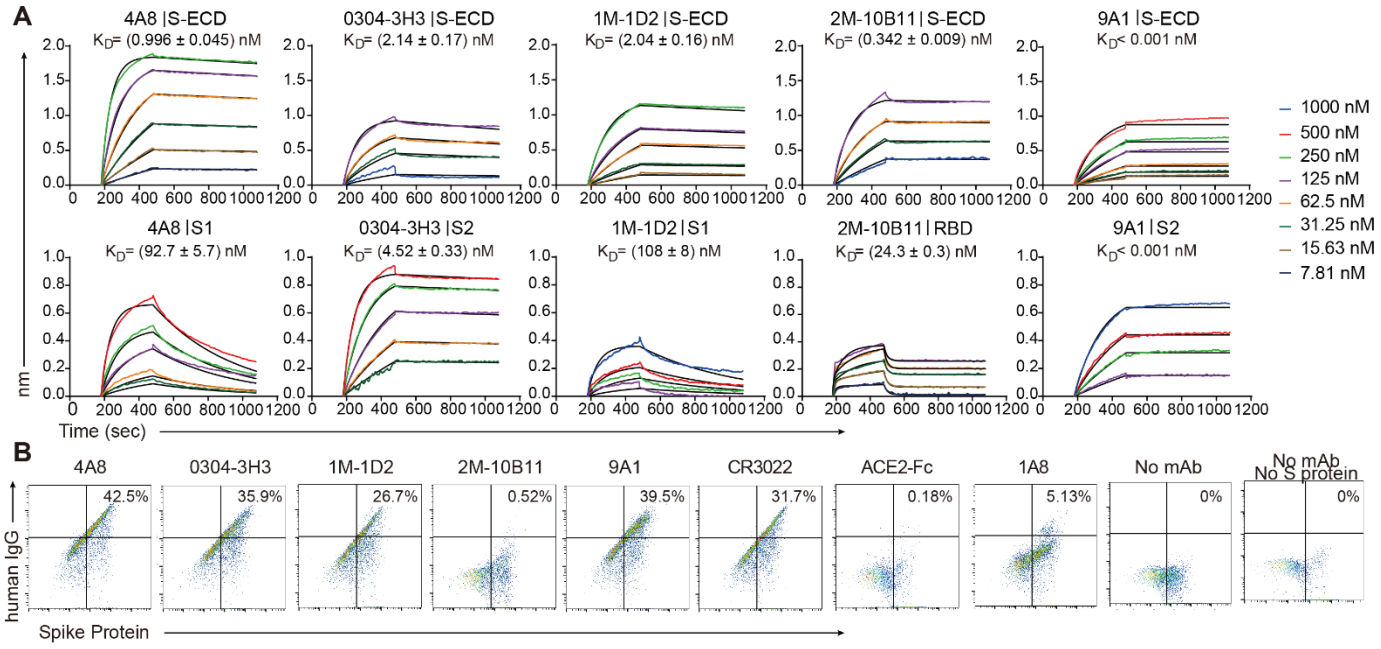

Fig. 4. 4A8 did not block the binding of Spike protein to ACE2 receptor. (**A**) BLI sensorgrams and kinetics of mAbs binding to S proteins. Global fitting curves were shown as black lines. The KD were calculated using a 1:1 binding model in Data Analysis Software 9.0, except for 2M-10B11 that uses heterogeneous ligand model due to avidity effect. (**B**) The binding of S protein to human ACE2 overexpressing 293T cells were determined by flow cytometry. Following the preincubation of S protein with each indicated mAb, the mAb-S mixtures were added to the ACE2-expressing cells. cells were stained with anti-human IgG FITC (mAb binding, x-axis) and anti-His (S binding, y-axis). Percentages of double positive cells were shown. Control mAb CR3022 and 1A8 were previously reported to bind SARS-CoV RBD and Marburg glycoprotein, respectively, and ACE2-Fc protein was a human ACE2 protein conjugated with human Fc.

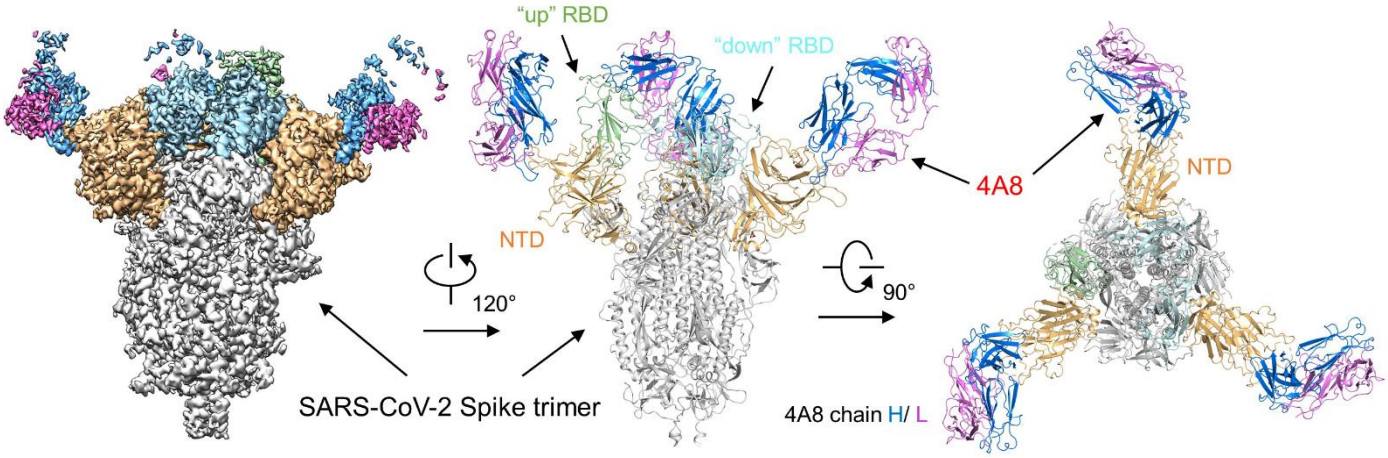

Fig. 5. Cryo-EM structure of the 4A8 and S-ECD complex. The domain-colored cryo-EM map of the complex is shown on the left, and two perpendicular views of the overall structure are shown on the right. The heavy and light chains of 4A8 are colored blue and magenta, respectively. The NTDs of the trimeric S protein are colored orange. The one "up" RBD and two "down" RBDs of trimeric S protein are colored green and cyan, respectively.

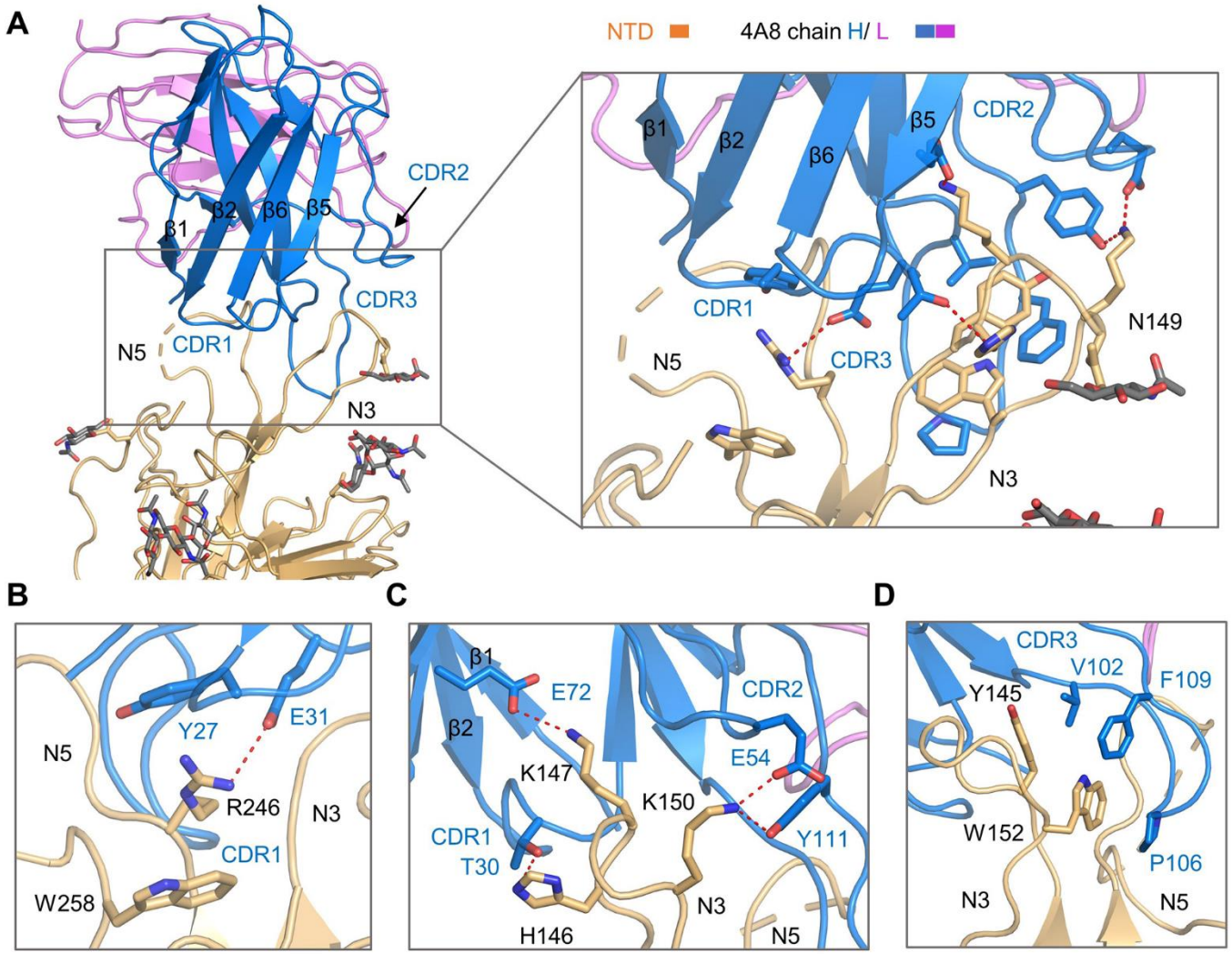

Fig. 6. Interactions between the NTD and 4A8. (**A**) Extensive hydrophilic interactions on the interface between NTD and 4A8. Only one NTD-4A8 is shown. (**B** to **D**) Detailed analysis of the interface between NTD and 4A8. Polar interactions are indicated by red, dashed lines. The residues involved in hydrophobic interactions are presented as spheres.